Korea-Australia Rheology Journal, 33(4), 357-366 (November 2021) www.springer.com/13367
DOI: 10.1007/s13367-021-0028-7

Morphology, electrical conductivity, and rheology of latex-based polymer/nanocarbon nanocomposites

Keon-Soo Jang, Hyo Yeol Yeom, Ju Won Park, Song Hee Lee and Seong Jae Lee*
Department of Polymer Engineering, The University of Suwon, 17, Wauan-gil, Bongdam-eup, Hwaseong, Gyeonggi 18323, Republic of Korea

(Received July 11, 2021; final revision received October 8, 2021; accepted October 16, 2021)

Nanocarbon materials are critical ingredients with unique properties in emerging materials. In this study, various carbon nanofillers, such as carbon nanotube (CNT), graphene oxide (GO), reduced GO wrapped by poly(styrene sulfonate) (PSS-RGO), and graphite nanoplatelet (GNP), were utilized to examine the effects of nanofiller types and surface treatments on the electrical and rheological properties of polystyrene (PS) nanocomposites prepared by latex-based process. The PS/CNT nanocomposites exhibited the most enhanced electrical and rheological properties among the composites evaluated. The PS/GO nanocomposites showed improved rheological properties and significantly increased electrical conductivity, despite the decrease in the intrinsic properties of graphene due to the change in hybridization from sp^2 to sp^3 by strong acid treatment. Interestingly, they exhibited higher conductivity than PS/PSS-RGO due to the higher graphene moiety and the thermal reduction of GOs during compression molding. The PS/GNP nanocomposites showed marginal enhancement because GNP is a larger aggregate of graphene layers bonded by van der Waals force. The results of this study on the electrical and rheological properties, surface modification, and size and dispersion of conductive nanofillers in an insulating polymer matrix are beneficial for the development and application of electrically conductive nanocomposites.

Keywords: nanocomposites, carbon nanofillers, latex-based process, electrical conductivity, rheological properties

1. Introduction

Various forms of natural and artificial composite materials have been extensively used. Currently, nanocomposites play a major role as functional materials for reinforcement and electrical conduction (Mezzenga and Ruokolainen, 2009). A considerable interest has arisen in fabrication methods of nanocomposites containing a polymer matrix and nanoscale fillers. These polymer nanocomposites can be facilely produced by the incorporation of nanofillers into a polymer matrix. Nanofillers are defined as fillers with at least one dimension measuring <100 nm. Nanofillers can substantially improve the optical, mechanical, magnetic, thermal and electrical properties of composites (Manias, 2007). The high specific surface area of nanofillers provides minimal disruption to the polymer matrix (Njuguna *et al.*, 2008). Nanofiller-based composites show superior reinforcement and functional enhancement over conventional microfiller-based composites (Šupová *et al.*, 2011). Polymers generally feature excellent processability but poor conductivity except for high-performance polymers and conjugated polymers. Electrically conductive polymer composites have been widely utilized for engineering applications such as electromagnetic interference shielding (Al-Saleh *et al.*, 2013), thermal interface materials (Shahil and Balandin, 2012), electrostatic discharge protection (Smith *et al.*, 2004), antistatic protection (Ma *et al.*, 2006), flexible optoelectronics and electronic devices (Wang *et al.*, 2008). The polymer nanocomposites with tunable electrical conductivity have shown increasing demand every year (Chizari *et al.*, 2017; Zhan *et al.*, 2017).

The electrical conductivity of polymer nanocomposites is highly dependent on the concentration of the conductive nanofiller (Zhan *et al.*, 2017). The percolation threshold of nanocomposites is defined as the theoretical nanofiller content required to provide the conducting path through the polymer matrix (Kalaitzidou *et al.*, 2007). At low nanofiller concentrations, the fillers are rarely connected to one another, thereby endowing the nanocomposites with an electrical conductivity as low as that of the pure insulating polymer matrix. The electrical conductivity of polymer nanocomposites rapidly increases by several orders of magnitude at the suitable nanofiller concentrations, causing the formation of a nanofiller-interconnected network structure throughout the matrix. This phenomenon enables the transition from an electrically insulating composite into a conductive composite (Sandler *et al.*, 2003). Above this electrical percolation threshold, addition of nanofillers into the polymeric matrix can improve the conductivity (Ma *et al.*, 2010). By contrast, the high loading of conductive nanofillers aggravates the mechan-

*Corresponding author; E-mail: sjlee@suwon.ac.kr

ical properties and pecuniary advantages of the polymer. Achieving the low electrical percolation threshold is a key factor to developing light-weight, economically viable next-generation conductive nanocomposites (Ramanathan *et al.*, 2008).

Considering that the conductivity of a composite is directly related to the nature of nanofillers, selecting developed nanofillers has been subjected to extensive research (Bagotia *et al.*, 2018; Zhang *et al.*, 2019). In most composite systems, inorganic fillers, such as metal nanomaterials, are incorporated into a polymeric matrix (Karttunen *et al.*, 2008; Sureshkumar *et al.*, 2015). Electrically conductive metallic polymer nanocomposites present certain disadvantages, such as corrosion, heaviness, high cost and processing difficulties due to metal materials (Al-Saleh, 2015). To overcome the hitches of metallic fillers, researchers have utilized carbonaceous fillers, including graphene (Li *et al.*, 2014), carbon nanotubes (CNTs) (Kim *et al.*, 2018), graphite nanoplatelets (GNPs) (Li and Zhong, 2011) and carbon black (Huang, 2002) with extraordinary properties, maintaining the electrical conductivities of polymer composites as high as the metallic composites. The overall properties of carbonaceous allotrope nanofiller-based composites strongly depend on the nature of host polymer, processing technique, size and volume fraction of nanofillers, degree of aggregation, and orientation of conductive network (Bhattacharya, 2016; Brigandi *et al.*, 2014). The rheological characteristics of nanocomposites also noticeably change through the incorporation of a high aspect-ratio carbonaceous nanofillers (Zhang *et al.*, 2008). Excellently conductive carbonaceous nanofillers are remarkably expensive. Hence, polymer nanocomposites with carbonaceous nanofiller are in their early stage of commercialization, and extensive effort is still needed to improve the overall outcome of conductive composites.

The simple mixing of nanosized carbon fillers with a polymer matrix is not a straightforward process due to poor dispersion of nanofillers. Predominantly, van der Waals force between carbon nanofillers leads to their agglomeration (Narh *et al.*, 2008). For example, the poor dispersion and weak interfacial adhesion between the graphene nanofiller and the polymer matrix result in agglomeration (Kuilla *et al.*, 2010). Graphene oxide (GO) is of eminent interest as an alternative form of atom-thick carbon scaffold nanofillers. GO contains a two-dimensional platelet-shaped sheet with abundant oxygen-rich functional groups (Stobinski *et al.*, 2014), which is hydrophilic but non-conductive; a reduction step is required to recover the electrically conductive properties. Using effective chemical reducing reagents and high-temperature reduction routes produce reduced GO, sacrificing hydrophilicity (Pei and Cheng, 2012). This phenomenon leads to the aggregation of reduced GO in the composites. To prepare agglomeration-free polymer nanocomposites, numerous methods, such as direct melt processing (Steurer *et al.*, 2009), coagulation (Ramanathan *et al.*, 2008), in-situ polymerization (Trujillo *et al.*, 2007), and latex blending (Wu and Chen, 2008), were introduced. Furthermore, modification of the conductive nanofiller surface with a conjugated polymer improves the dispersion quality of the nanocomposite while maintaining its intrinsic properties. Covalent modifications substantially reduce electrical conductivity by the change from sp^2 to sp^3 structure, whereas physical modifications such as π-π interactions between graphene and conjugated polymers preserve sp^2 hybridization orbitals (Song *et al.*, 2021). For instance, poly(styrene sulfonate) (PSS)-stabilized graphene platelet nanofiller (Yoo *et al.*, 2014) and poly(N-vinylpyrrolidone)-grafted polymer (Long *et al.*, 2013) decreased the agglomeration of nanofillers. Another major issue in preparing carbonaceous nanocomposite is the usage of organic solvents (Compton and Nguyen, 2010), which are harmful to the environment and limit the processing temperature range.

Latex-based process is one of the protocols to overcome aggregation, which allows the straightforward incorporation of predominantly individual nanofillers into a highly viscous polymer matrix (Mechrez *et al.*, 2014). This process is involved with mixing a stabilized aqueous nanofiller dispersion with a polymer latex, followed by freeze-drying and compression molding (Tkalya *et al.*, 2010; Regev *et al.*, 2004). Latex-blended nanocomposites also show low percolation threshold and good electrical conductivity due to good dispersibility. In addition to facile incorporation, the latex process is environmentally friendly, versatile, reproducible, and reliable. This process requires no toxic solvents and can be easily scaled up with high dispersion qualities. It can be easily extended to various polymers synthesized by emulsion polymerization (Cai and Song, 2008; Dufresne *et al.*, 2002; Grossiord *et al.*, 2005).

Conductivity varies with many factors, such as the thickness of samples, polymer matrix type, fabrication method, and processing conditions. To further understand and develop the carbonaceous polymer nanocomposites, comparative studies based on different carbon nanoallotropes are required. In view of the limited comparative studies, the present work focused on nanocomposites consisting of polystyrene (PS) and four different conductive nanofillers, such as CNT, GO, reduced GO wrapped by PSS (PSS-RGO), and GNP.

2. Experimental

2.1. Materials

Potassium persulfate (KPS, 30 wt% in H_2O), sodium dodecylsulfate (SDS), hydrazine monohydrate, graphite (average particle size of < 20 μm), and PSS (70,000 g/mol) were purchased from Sigma Aldrich (St. Louis, MO,

USA). Styrene monomer (Samchun Chemical, Seoul, Korea) was purified by vacuum distillation prior to use. Deionized (DI) water was purified by Option-Q (PureLab, ELGA, High Wycombe, UK). H_2SO_4, $KMnO_4$, H_2O_2, HCl, and ethanol were obtained from Samchun Chemical. Multi-walled CNT (NC-7000) was purchased from Nanocyl (Sambreville, Belgium). P_2O_5 was obtained from Kanto Chemical (Tokyo, Japan). GNP (xGnP M-5) was purchased from XG Science (Lansing, MI, USA). The SEM images of CNTs and GNPs are shown in Fig. 1.

2.2. Synthesis of monodispersed PS particles

Monodispersed PS particles with an average diameter of ca. 500 nm were synthesized via emulsifier-free emulsion polymerization (Song *et al.*, 2021). A total of 43.2 mL ethanol and 360 mL DI water were placed in a three-neck double-jacket Pyrex reactor under N_2 atmosphere. A total of 40 mL styrene and 0.3676 g KPS (water-soluble initiator) were added to the reactor. Polymerization was carried out at 70°C for 24 h at a stirring speed of 300 rpm. The PS particles were purified by centrifugation and washing cycles with ethanol and DI water.

2.3. Preparation of GO

GO sheets were synthesized via graphite oxidation based on modified Hummers method (Kovtyukhova *et al.*, 1999). For preoxidation, 2.0 g graphite flake was added into the solution mixture comprising 5.0 mL H_2SO_4, 0.8 g $K_2S_2O_8$, and 1.0 g P_2O_5 and the whole solution was stirred for 6 h. Afterward, the suspended mixture was diluted with DI water and centrifuged repeatedly to achieve neutral conditions. Then, it was vacuum dried after glass-filtering the suspension. For oxidation, 2.0 g graphite prepared at the preoxidation stage was added slowly to the cooled solution (0°C in an ice bath) of 46 mL H_2SO_4 and 6.0 g $KMnO_4$ to keep the temperature of the mixture below 20°C. Then, the mixture was heated up to 35°C and stirred for 2 h. Subsequently, 92 mL DI-water and 5.0 mL H_2O_2 were added to the mixture. When the color of the mixture transitioned to bright yellow, 375 mL DI water and 125 mL of 5 wt% HCl aqueous solution were added and stirred for 1 h. Subsequently, the mixture was diluted with DI-water and centrifuged to neutral condition. The resultant GO nanosheets were obtained by filtering and drying.

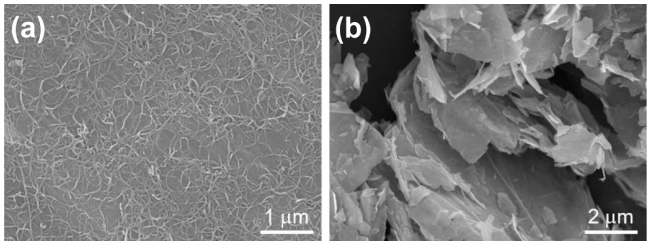

Fig. 1. SEM images of commercial carbon nanofillers used in this study: (a) CNTs (NC-7000, Nanocyl) and (b) GNPs (M-5, xGnP).

2.4. Preparation of PSS-RGO

PSS-RGO sheets were prepared by the modification of previously reported procedures involving the chemical reduction of aqueous GO suspensions (Stankovich *et al.*, 2006). The GO suspensions (200 mL, 1 g/L) were sonicated for 30 min using an ultrasonication bath (Branson 3510, Branson Ultrasonics Co., Danbury, CT, USA), and then 2 g PSS was added and dispersed at 50°C for 4 h. Afterward, 4 mL hydrazine monohydrate was added and heated under reflux at 100°C for 24 h. Excess PSS and hydrazine monohydrate were removed by repeated filtration (Nylon filter, pore size of <0.2 μm) and washing cycles. Finally, PSS-RGO sheets were obtained by drying the residual solid at 80°C for 2 h.

2.5. Preparation of PS/nanofiller nanocomposites by latex-based process

PS/GO nanocomposites were fabricated through the following procedure. GO nanosheets were dispersed in DI water and sonicated at 20 W for 30 min with an ultrasonic probe (VC 505, Sonics & Materials Inc., Newtown, CT, USA). The GO aqueous suspension was mixed with the synthesized PS particles and ultrasonicated again for 30 min with the probe. The homogeneously dispersed PS/GO mixture was abruptly frozen with liquid nitrogen, after which the aqueous moiety in the frozen mass was removed by freeze-drying (FD-1000, EYELA, Tokyo Rikakikai Co., Tokyo, Japan). Finally, the freeze-dried PS/GO nanocomposite powders were compression-molded into 1-2 mm thick disk-type samples with a diameter of 25 mm at 180°C for 5 min. The fabrication procedure for the PS/PSS-RGO nanocomposites was the same as that for the above GO nanosheets. For the preparation of PS/CNT or PS/GNP nanocomposites, surfactant SDS was added to

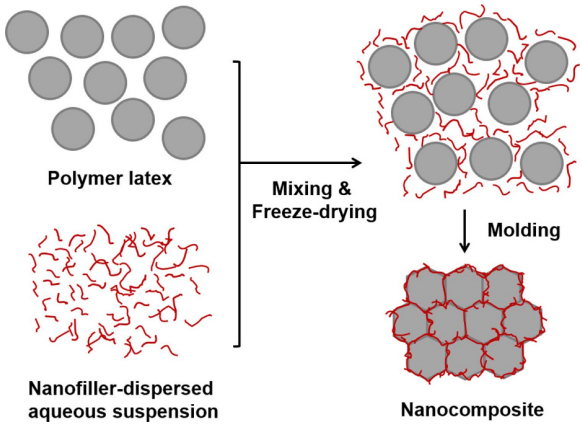

Fig. 2. (Color online) Procedure for fabrication of PS/nanofiller nanocomposite by latex-based process.

aid the aqueous dispersion of CNT or GNP. The weight ratios of SDS:CNT and SDS:GNP were 2 and 1, respectively. Figure 2 shows a schematic diagram of the procedure for the preparation of the PS/nanofiller nanocomposites by latex-based process.

2.6. Characterization

The size and morphology of PS particle, carbon nanofillers, PS/nanofiller freeze-dried powder, and fracture surface of nanocomposites were investigated with field-emission scanning electron microscopy (FE-SEM, JSM 6700F, Jeol, Akishima, Japan). Thermogravimetric analysis (TGA, STA 409, Netzsch, Selb, Germany) of graphene nanofillers was carried out at a heating rate of 10°C/min under N_2 from room temperature to 600°C. Fourier transform infrared (FT-IR) spectroscopy was performed on a Spectrum Two (Perkin Elmer, Waltham, MA, USA). Powder X-ray diffraction (XRD, D8 Advance, Bruker, Billerica, MA, USA) was carried out using a diffractometer with CuKα radiation. X-ray photoelectron spectroscopy (XPS) measurements were carried out on a Sigma Probe (Thermo Fisher Scientific, Waltham, MA, USA).

The electrical properties of the nanocomposites were measured with a picoammeter (Keithley 6487, Keithley Instruments, Solon, OH, USA) and a digital multimeter (Fluke 189, Fluke Corp., Everett, WA, USA). After applying silver paste (Elcoat P-100, CANS, Tokyo, Japan) on both sides of the specimens, the resistance of the sample was measured. The electrical conductivity was calculated from the following equation,

$$\sigma = 1/\rho = d/RS \ , \tag{1}$$

where σ, ρ, R, d, and S denote the electrical conductivity, resistivity, resistance, sample thickness, and sample cross-sectional area, respectively.

The rheological properties of the nanocomposites were investigated with a rotational rheometer (MCR 300, Anton Paar, Graz, Austria) in small-amplitude oscillatory shear mode using parallel plate geometry. After confirming that the amplitude was recorded within the linear viscoelastic range, frequency sweeps between 0.03 and 100 s^{-1} were performed at a strain amplitude of 3% throughout the measurements. All measurements were conducted at 210°C.

3. Results and Discussion

The morphology of polymer nanocomposites is important in predicting and correlating various properties. Nanocomposites are typically subjected to morphological examination by SEM. The properties of nanocomposites are determined by the types, size, concentration, and dispersion of the nanofillers and molecular weight (MW) of the polymers. For instance, the MW of PS increases with decreasing size of PS particles, thereby influencing morphologies and mechanical properties (Paine *et al.*, 1990). Herein, considering that the characteristics of the synthesized monodispersed PS particles were identical, the properties of nanocomposites can be influenced by the types of nanofiller and the associated polydispersity. Figure 3 shows the nanocomposite powder mixtures consisting of monodispersed PS particles and each nanofiller. As can be seen in Fig. 3(a), CNTs are well-dispersed in PS particles. The SDS molecules adsorbed on CNT attenuate the aggregation of CNT nanofillers in the aqueous solution. However, when the surface-to-surface interparticle distance between the CNT nanofillers becomes smaller than the diameter of SDS micelle, the micelle is excluded with depletion volume, resulting in CNT aggregation due to capillary forces (Bonard *et al.*, 1997). Figures 3(b) and 3(c) display the PS/GO and PS/PSS-RGO nanocomposite powder mixtures, respectively. GO and PSS-RGO with platy structures were coated on the PS particles with nanofiller connections. GO was exfoliated with good dispersity due to the combination of oxidation and ultrasonication during preparation. In addition, freeze-drying impeded aggregation and phase separation during drying. The morphology of PS/PSS-RGO was analogous to that of PS/GO. The hydrophilic PSS was attached to the GO surface in aqueous solution, and then PSS-GO was chemically reduced with hydrazine monohydrate while preventing the aggregation of GO platelets (Stankovich *et al.*, 2006; Jo *et al.*, 2011). This delicate process enhanced the dispersion and chemical reduction at the same time. By contrast, GNP was thicker and broader (Figs. 1(b) and 3(d)) than GO and PSS-RGO although these three nanofillers featured similar tabular structures. Thus, PS particles were adsorbed on the partially aggregated GNPs, limiting the

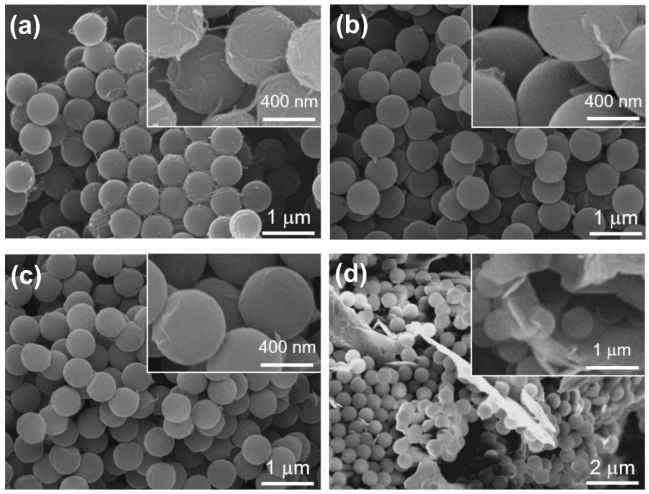

Fig. 3. SEM images of freeze-dried PS/nanofiller powder mixture: (a) 3 wt% CNT, (b) 3 wt% GO, (c) 3 wt% PSS-RGO, and (d) 15 wt% GNP.

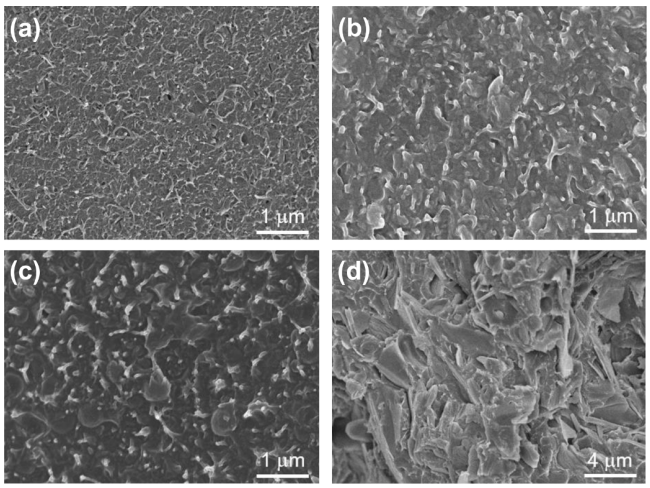

Fig. 4. SEM images of fracture surfaces of PS/nanofiller nanocomposites: (a) 3 wt% CNT, (b) 3 wt% GO, (c) 3 wt% PSS-RGO, and (d) 15 wt% GNP.

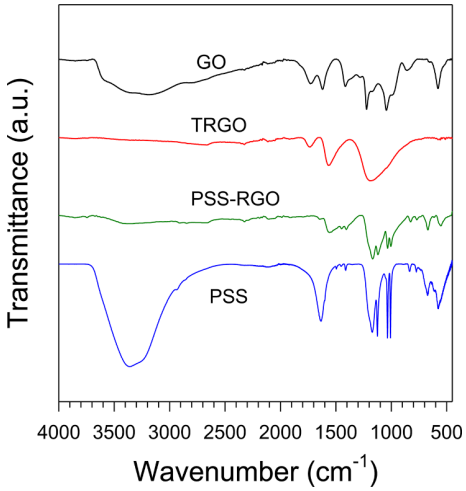

Fig. 6. (Color online) FT-IR spectra of GO, TRGO, PSS, and PSS-RGO.

homogenous nanolevel dispersion. Figure 4 shows the cryogenic fracture surfaces of nanocomposites, which were compression-molded with the powder mixture at 180°C for 5 min. The nanofiller dispersity of the PS/GNP nanocomposite was poorer than that of the PS/CNT, PS/GO, and PS/PSS-RGO nanocomposites.

XRD was utilized for the GO and GNP to probe their crystallographic difference (Fig. 5). Given that GNPs originated from graphite, the crystallographic distance (3.3 Å, $2\theta = 26.70°$) between (002) GNP crystal planes was analogous to that (3.35 Å) for graphite, indicating their identical crystal structure. A peak at $2\theta = 11.13°$ was observed for GO, representing 7.9 Å of the distance between the (002) GO crystal planes. This increment in distance was observed because the oxygen-based functional units generated during oxydation spread in the space between the GO crystal planes (McAllister *et al.*, 2007). This phenomenon proved that GO was produced by graphite oxidation.

FT-IR has been routinely performed to examine surface-modified GOs. Figure 6 shows the FT-IR spectra of GO, thermally reduced GO (TRGO, treated at 180°C for 5 min.), and chemically reduced GO (PSS-RGO). GO exhibited various characteristic peaks at 3400, 1735, 1622, 1414, and 1228/1045 cm^{-1} for –OH, C=O (carbonyl), C=C (aromatic), C–O (carboxylic), and C–O (epoxy), respectively. For TRGO, the peaks for most functional moieties including oxygen disappeared or decreased, whereas the peak at 1600 cm^{-1} for aromatic C=C relatively increased. The peak for epoxide was still observed. These results suggested that most –OH and –COOH groups were reduced to C=C groups, whereas the reduction of epoxide was not completely achieved during mild heat treatment at 180°C. PSS-RGO showed the characteristic peaks at 1190/1128/1039/1005 cm^{-1} as absorption frequencies of the $-SO_3^-$ moiety in PSS (Sun *et al.*, 2014). FT-IR analysis confirmed that GO was substantially thermally reduced and that PSS-RGO was encapsulated by PSS.

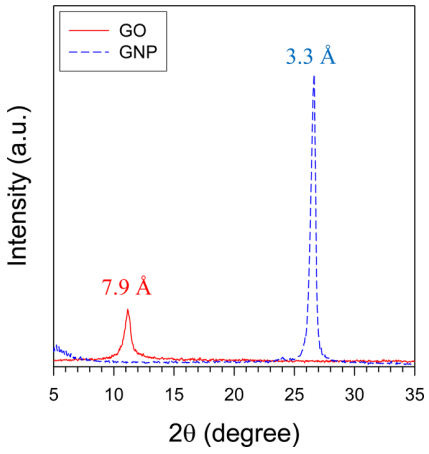

Fig. 5. (Color online) XRD patterns of GO and GNP.

XPS was utilized to further confirm the synthesis of carbon nanofillers, such as GNP, GO, TRGO, and PSS-RGO (Fig. 7). For GNP, the peaks at approximately 284.5, 286.8 and 288.5 eV were assigned to C–C/C=C, C–O, and C=O, respectively. The intense peak at 284.5 eV was observed for all samples. For GO, the second intense peak at 286.8 eV (C–O) with a shoulder at 288.5 eV (C=O) appeared due to the synthesis via graphitic oxidation. The spectra of TRGO showed an intense peak at 284.5 eV accompanied by some shoulders at higher binding energies due to the presence of oxygen linkages. The atomic C/O ratio of GO and TRGO increased from 2.25 to 2.76 when GO was thermally treated at 180°C, which is similar to the cases of RGO (Jo *et al.*, 2011; Paredes *et al.*, 2008). The thermal treatment for GO partially recovered the sp^2 structure, thereby possibly enhancing the electrical properties. For PSS-RGO, the strong peak of C–C/C=C appeared as a

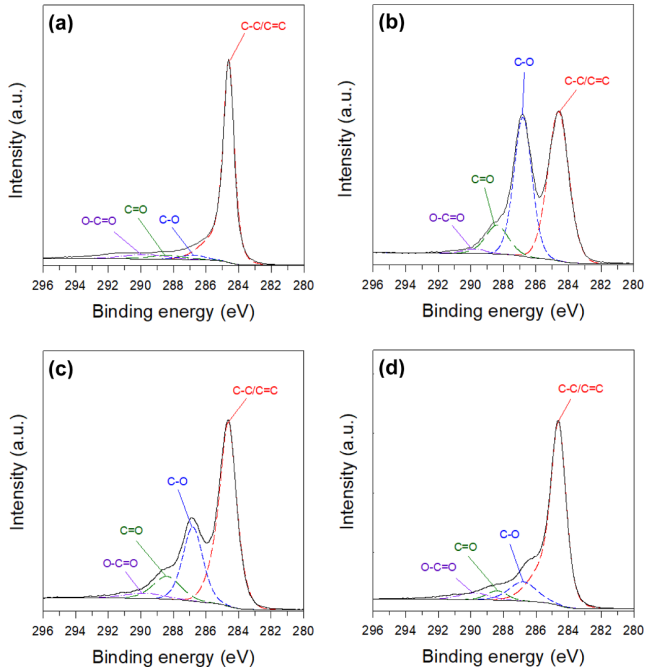

Fig. 7. (Color online) C 1s XPS spectra with deconvoluted peaks: (a) GNP, (b) GO, (c) TRGO, and (d) PSS-RGO.

result of chemical reduction of GO, and the C/O ratio increased to 4.14. The overall shape and peak positions of corresponding bonds were maintained after adding PSS, which indicates the strong π-π interactions and good compatibility between RGO and PSS chains. Compared to TRGO, the chemically reduced PSS-RGO showed weaker shoulders for oxygen-containing binding energies, indicating that PSS-RGO was reduced more strongly than TRGO.

TGA is a facile method to predict chemical degradation, surface modification, and chemically structural change by detecting the weight loss of a material. As shown in Fig. 8, the residual weight of CNT showed 95.7 wt% at 600°C,

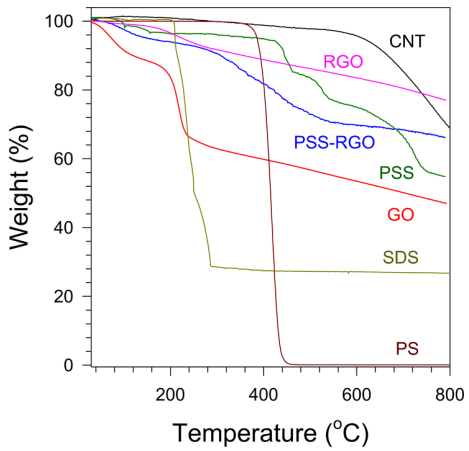

Fig. 8. (Color online) TGA of CNT, GO, RGO, PSS, PSS-RGO, SDS, and PS.

but decreased to 68.9 wt% at 800°C, indicating that it was thermally stable up to 600°C. The weight of GO started to decrease at 200°C due to the decomposition of labile oxygen-containing functional groups, yielding CO, CO_2 and H_2O. The GO weight of 46.8 wt% remained at 800°C. The weights of residual compounds for PSS and PSS-RGO at 800°C were 54.5 and 65.6 wt%, respectively. Compared with the weight loss of GO at 220°C, PSS-RGO did not follow this trend, indicating that it was almost completely reduced during chemical reduction. The GO chemically reduced by hydrazine monohydrate (RGO) was also analyzed to determine the PSS moiety in PSS-RGO. The weight of RGO was 76.7 wt% at 800°C. From the residual weights of RGO, PSS and PSS-RGO, the PSS content of PSS-RGO was determined to be about 50 wt%, indicating that RGO was encapsulated with PSS chains of equal weight. PS showed a drastic weight loss in the range of 400-450°C, and weights less than 0.1 wt% were remained at 800°C. The surfactant SDS showed a sharp decrease of weight in the range of 200-300°C, but 26.7 wt% still remained at 800°C due to undecomposed S- and Na-binding compounds.

The electrical properties of nanocomposites consisting of conductive nanofillers and insulating polymers are an attractive phenomenon giving high electrical conductivity obtained by the incorporation of a small amount of nanofillers into a polymeric matrix. In addition to type, aspect ratio, and concentration of nanofillers, the dispersion of nanofillers in a polymer matrix strongly influences the electrical conductivity of nanocomposites (Du *et al.*, 2004; Kim *et al.*, 2019). Figure 9 shows that the electrical conductivities of nanocomposites were highly determined by the nanofiller content and types. Their electrical conductivities were as low as that of the pristine PS (ca. 10^{-11} S/

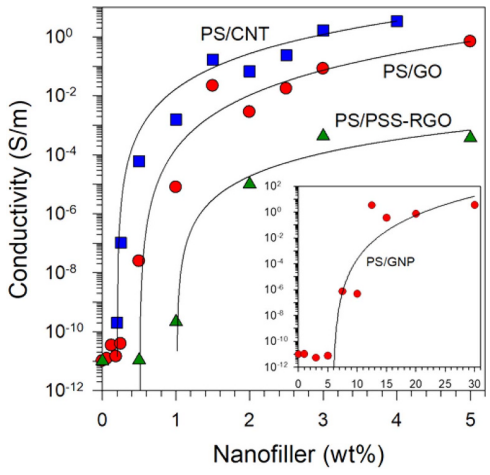

Fig. 9. (Color online) Electrical conductivity of PS/nanofiller (PS/CNT, PS/GO, PS/PSS-RGO, and PS/GNP) nanocomposites. The solid line represents a regression fit to the power-law relation shown in Eq. (2).

Table 1. Summary of the experimental parameters of conductive nanocomposites, where m_c, b and σ_{max} stand for electrical percolation threshold, critical exponent, and maximum electrical conductivity

Nanofiller	m_c [wt%]	b	σ_{max} [S/m]
CNT	0.23	3.34	3.42E+0 (4 wt%)
GO	0.50	3.82	6.93E-1 (5 wt%)
PSS-RGO	1.01	2.60	6.92E-4 (5 wt%)
GNP	5.82	6.37	1.66E+1 (30 wt%)

m), that is, below the electrical percolation threshold of each composite. Above this threshold, the conductivities significantly increased. These phenomena represented the formation of conductive networks, which was consistent with the SEM studies. The electrical behavior of polymer nanocomposites complied well with the percolation theory predictions despite the possible barriers, such as surfactant molecules, monolayer coating, and gaps in the composites (Balberg, 2009; Wu *et al.*, 2006). The electrical percolation threshold is typically determined by a power–law relationship between electrical conductivity and nanofiller loading, as follows,

$$\sigma \propto (m - m_c)^b, \tag{2}$$

where σ, m, m_c, and b denote the electrical conductivity of nanocomposite, weight percent of nanofiller, electrical percolation threshold, and critical exponent related to the system dimension, respectively. Table 1 summarizes the experimental parameters of nanocomposites, regression-fitted by Eq. (2). The critical exponent b is an index correlated with the microstructural properties of composites (Hu *et al.*, 2006). The b value for polymer composites with globular fillers is generally ca. 1.9, and that with fibrous fillers is above 2 (Weber and Kamal, 1997).

The electrical conductivity of the PS/GO nanocomposite was higher than anticipated, and such result was caused by the partially recovered graphene structure due to thermal reduction. The thermal reduction of GO may occur during composite fabrication such as high temperature melt blending and compounding. PS/PSS-RGO showed a lower electrical conductivity than PS/GO, despite their similar morphologies (Figs. 3 and 4) and rheological properties (Fig. 10). Whereas PSS-RGO was highly chemically reduced as seen in Fig. 7(c), the electrically insulating PSS impeded the electrical network and the graphene portion of PSS-RGO was lower than that of TRGO as mentioned in the TGA results. Thus, the two negative factors for electrical conductivity enhancement prevailed over the positive factors by chemical reduction. In terms of PS/CNT nanocomposite, the adsorbed SDS on CNT surfaces

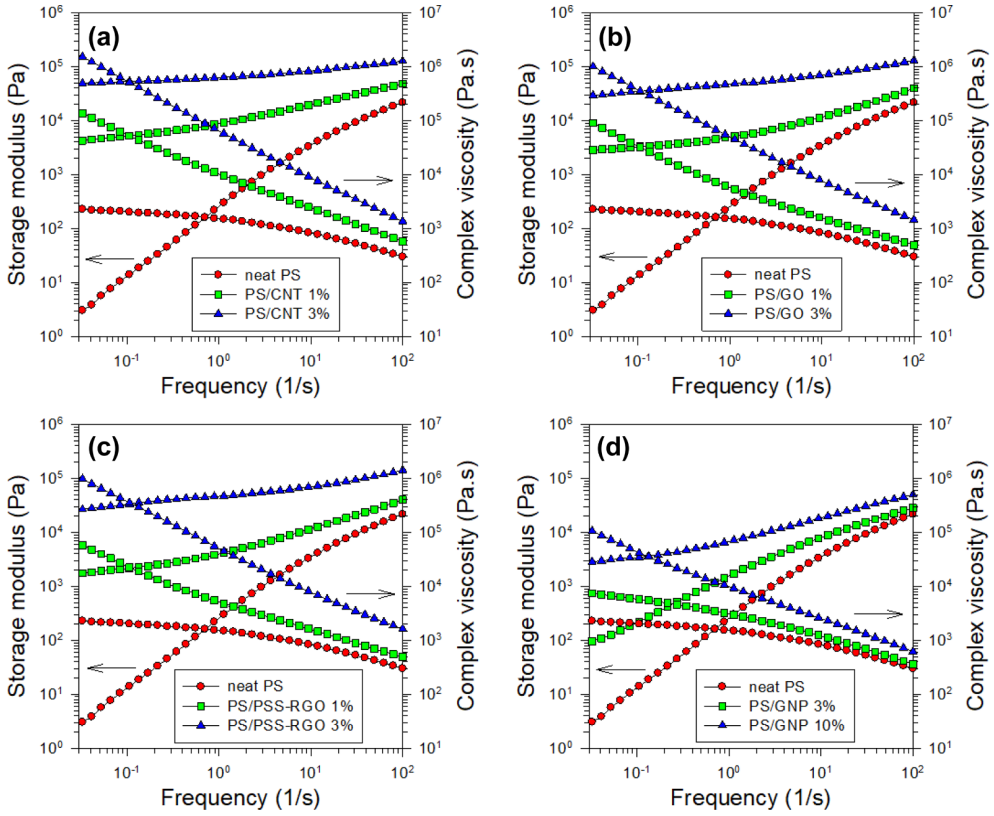

Fig. 10. (Color online) Rheological properties (storage modulus and complex viscosity) of PS/nanofiller composites: (a) PS/CNT, (b) PS/GO. (c) PS/PSS-RGO, and PS/GNP nanocomposites.

improved the aqueous dispersion. After achieving stable dispersion in the matrix, the low-MW and heat-sensitive SDS can be easily desorbed from the CNT surfaces during melt processing, leading to the sturdy CNT-CNT network formation with the highest electrical conductivity. Moreover, the electrical conductivity of PS/CNT must be higher than that of PS/GO because of the GO damaged by acid treatment, incomplete reduction of GO, and high aspect ratio of CNT. The PS/GNP nanocomposite showed an electrical conductivity as high as that of PS/CNT because of the well-developed sp^2 structure and no oxidation step as in the case of CNT, thereby maintaining the intrinsic properties. However, the electrical percolation threshold of PS/GNP was considerably higher than that of PS/CNT because of much bigger size and poorer dispersity. Thus, in terms of the electrical percolation threshold, PS/CNT exhibitd a superior performance, whereas PS/GNP showed the poorest. For the electrical conductivity, PS/PSS-RGO was the lowest.

The rheological properties of nanocomposites is highly correlated with various factors, including particle dispersion, viscoelasticity, mixing behavior, productivity rate, and energy consumption; their applications range from paints to electronics (Nikolić *et al.*, 2011; Lee *et al.*, 1999). Accordingly, the nanocomposites fabricated in this study were subjected to rheological investigation for the dispersion characteristics, microstructural transition, and viscoelasticity. Figure 10 shows the rheological properties of the compression-molded nanocomposites. The complex viscosity of the pristine PS showed a Newtonian behavior at low frequencies and a shear thinning behavior at high frequencies, which is similar to typical polymer melts. However, the slope of complex viscosity versus frequency for nanocomposites became steep because of the incorporation of nanofillers, such as CNT, GO, PSS-RGO, and GNP into the PS matrix. By contrast, the slope of storage modulus versus frequency became gentle with increasing nanofiller content. The infiltration of nanofillers into the PS matrix enhanced the storage modulus. The storage modulus (G') of nanocomposites rarely changed as a function of frequency (ω), which was in contrast to those of the pure PS. For monodispersed MW polymers, a terminal behavior ($G' \sim \omega^2$) appears at low frequency ranges. This phenomenon is suppressed by increasing nanofiller loading because the nanofiller network structure hindered the relaxation behavior of polymers, thereby showing solid-like characteristics instead of liquid-like characteristics (Du *et al.*, 2004). However, the rheological properties of the nanocomposites at high frequencies are approaching those of neat PS. The physical network structure between nanofillers was destroyed due to high frequency-induced strong shear force. Thus, the rheological properties were influenced by the polymer matrix rather than the nanofillers, leading to only a slight increment in rheological properties in the high frequency ranges as a function of nanofiller loading.

In the nanocomposites, except for the PS/GNP nanocomposite, the rheological properties were significantly increased at 1 wt% addition of nanofillers. Above 1 wt%, the rheological behavior marginally changed because the rheological network structure was already built below 1 wt% caused by excellent dispersion (Du *et al.*, 2004; Hu *et al.*, 2006), which indicates the rheological percolation threshold is lower than 1 wt%. The PS/CNT nanocomposite in Fig. 10(a) showed the highest rheological properties because of the SDS-triggered homogeneous dispersion, high aspect ratio, and no chemical damage in CNT. The rheological properties of the PS/PSS-RGO nanocomposite shown in Fig. 10(c) were almost identical to the PS/GO counterpart shown in Fig. 10(b). Considering that the graphene portion of PSS-RGO was about half of that of GO, it is speculated that the PSS-RGO nanofiller was well dispersed in the matrix and the PSS chains surrounding the GO also actively interacted with the matrix PS chains. However, the rheological properties of 10 wt% PS/GNP given in Fig. 10(d) showed a smaller increase compared with those of 3 wt% PS/GO due to the substantially larger size and lower dispersibility of GNPs in the PS matrix.

4. Conclusions

We examined the effects of carbon nanofillers (*i.e.*, CNT, GO, PSS-RGO, and GNP) in the PS matrix on various properties, especially electrical and rheological properties. The nanocomposites were fabricated by the latex-based process followed by compression molding. Chemical analysis of nanofillers was performed by FT-IR, XRD, XPS, and TGA. GO was partially thermally reduced through heat treatment upon molding, thereby leading to partial recovery of inherent graphene structure with enhanced electrical properties. According to SEM images, and electrical and rheological properties, the uniform dispersion of nanofillers (CNT, GO, and PSS-RGO) in the PS matrix was confirmed, whereas the poor dispersion of GNP was observed. The electrical percolation thresholds of nanocomposites containing CNT, GO, and PSS-RGO reached lower than 1 wt%. The electrical percolation threshold of PS/CNT was the lowest (0.25 wt%) among all the samples, whereas that of PS/GNP was over 5.8 wt% due to the poorest dispersity of GNP in the PS matrix. Despite the highest electrical percolation threshold, the PS/GNP at higher GNP contents exhibited fairly good electrical conductivity. The results of this study can be beneficial for the applications of electrically conductive nanocomposites.

Acknowledgments

The authors gratefully acknowledge the National Research Foundation of Korea (NRF), funded by the Korea government (MSIT) (NRF-2018R1A5A1024127 and NRF-2021R1F1A1063116).

References

Al-Saleh, M.H., 2015, Influence of conductive network structure on the EMI shielding and electrical percolation of carbon nanotube/polymer nanocomposites, *Synth. Met.* **205**, 78-84.

Al-Saleh, M.H., W.H. Saadeh, and U. Sundararaj, 2013, EMI shielding effectiveness of carbon based nanostructured polymeric materials: a comparative study, *Carbon* **60**, 146-156.

Bagotia, N., V. Choudhary, and D.K. Sharma, 2018, A review on the mechanical, electrical and EMI shielding properties of carbon nanotubes and graphene reinforced polycarbonate nanocomposites, *Polym. Adv. Technol.* **29**, 1547-1567.

Balberg, I., 2009, Tunnelling and percolation in lattices and the continuum, *J. Phys. D: Appl. Phys.* **42**, 064003.

Bhattacharya, M., 2016, Polymer Nanocomposites–A comparison between carbon nanotubes, graphene, and clay as nanofillers, *Materials* **9**, 262.

Bonard, J.-M., T. Stora, J.-P. Salvetat, F. Maier, T. Stöckli, C. Duschl, L. Forró, W.A. de Heer, and A. Châtelain, 1997, Purification and size-selection of carbon nanotubes, *Adv. Mater.* **9**, 827-831.

Brigandi, P.J., J.M. Cogen, and R.A. Pearson, 2014, Electrically conductive multiphase polymer blend carbon-based composites, *Polym. Eng. Sci.* **54**, 1-16.

Cai, D. and M. Song, 2008, Latex technology as a simple route to improve the thermal conductivity of a carbon nanotube/polymer composite, *Carbon* **46**, 2107-2112.

Chizari, K., M. Arjmand, Z. Liu, U. Sundararaj, and D. Therriault, 2017, Three-dimensional printing of highly conductive polymer nanocomposites for EMI shielding applications, *Mater. Today Commun.* **11**, 112-118.

Compton, O.C. and S.T. Nguyen, 2010, Graphene oxide, highly reduced graphene oxide, and graphene: Versatile building blocks for carbon-based materials, *Small* **6**, 711-723.

Du, F., R.C. Scogna, W. Zhou, S. Brand, J.E. Fischer, and K.I. Winey, 2004, Nanotube networks in polymer nanocomposites: rheology and electrical conductivity, *Macromolecules* **37**, 9048-9055.

Dufresne, A., M. Paillet, J.L. Putaux, R. Canet, F. Carmona, P. Delhaes, and S. Cui, 2002, Processing and characterization of carbon nanotube/poly(styrene-co-butyl acrylate) nanocomposites, *J. Mater. Sci.* **37**, 3915-3923.

Grossiord, N., J. Loos, and C.E. Koning, 2005, Strategies for dispersing carbon nanotubes in highly viscous polymers, *J. Mater. Chem.* **15**, 2349-2352.

Hu, G., C. Zhao, S. Zhang, M. Yang, and Z. Wang, 2006, Low percolation thresholds of electrical conductivity and rheology in poly(ethylene terephthalate) through the networks of multi-walled carbon nanotubes, *Polymer* **47**, 480-488.

Huang, J.-C., 2002, Carbon black filled conducting polymers and polymer blends, *Adv. Polym. Technol.* **21**, 299-313.

Jo, K., T. Lee, H.J. Choi, J.H. Park, D.J. Lee, D.W. Lee, and B.-S. Kim, 2011, Stable aqueous dispersion of reduced graphene nanosheets via non-covalent functionalization with conducting polymers and application in transparent electrodes, *Langmuir* **27**, 2014-2018.

Kalaitzidou, K., H. Fukushima, and L.T. Drzal, 2007, A new compounding method for exfoliated graphite–polypropylene nanocomposites with enhanced flexural properties and lower percolation threshold, *Compos. Sci. Technol.* **67**, 2045-2051.

Karttunen, M., P. Ruuskanen, V. Pitkänen, and W.M. Albers, 2008, Electrically conductive metal polymer nanocomposites for electronics applications, *J. Electron. Mater.* **37**, 951-954.

Kim, J.H., J.-Y. Hwang, H.R. Hwang, H.S. Kim, J.H. Lee, J.-W. Seo, U.S. Shin, and S.-H. Lee, 2018, Simple and cost-effective method of highly conductive and elastic carbon nanotube/polydimethylsiloxane composite for wearable electronics, *Sci. Rep.* **8**, 1375.

Kim, J.M., K.-S. Jang, and S.J. Lee, 2019, Electrically conductive polystyrene nanocomposites incorporated with aspect ratio-controlled silver nanowires, *J. Appl. Polym. Sci.* **136**, 47927.

Kovtyukhova, N.I., P.J. Ollivier, B.R. Martin, T.E. Mallouk, S.A. Chizhik, E.V. Buzaneva, and A.D. Gochinskiy, 1999, Layer-by-layer assembly of ultrathin composite films from micron-sized graphite oxide sheets and polycations, *Chem. Mater.* **11**, 771-778.

Kuilla, T., S. Bhadra, D. Yao, N.H. Kim, S. Bose, and J.H. Lee, 2010, Recent advances in graphene based polymer composites, *Prog. Polym. Sci.* **35**, 1350-1375.

Lee, J.-D., J.-H. So, and S.-M. Yang, 1999, Rheological behavior and stability of concentrated silica suspensions, *J. Rheol.* **43**, 1117-1140.

Li, B. and W.-H. Zhong, 2011, Review on polymer/graphite nanoplatelet nanocomposites, *J Mater Sci.* **46**, 5595-5614.

Li, Y., Y.A. Samad, K. Polychronopoulou, S.M. Alhassan, and K. Liao, 2014, Highly electrically conductive nanocomposites based on polymer infused graphene sponges, *Sci. Rep*. **4**, 4652.

Long, G., C. Tang, K. Wong, C. Man, M. Fan, W. Lau, T. Xu, and B. Wang, 2013, Resolving the dilemma of gaining conductivity but losing environmental friendliness in producing polystyrene/graphene composites via optimizing the matrix-filler structure, *Green Chem.* **15**, 821-828.

Ma, C.-C.M., Y.-J. Chen, and H.-C. Kuan, 2006, Polystyrene nanocomposite materials–Preparation, mechanical, electrical and thermal properties, and morphology, *J. Appl. Polym. Sci*. **100**, 508-515.

Ma, P.-C., N.A. Siddiqui, G. Marom, and J.-K. Kim, 2010, Dispersion and functionalization of carbon nanotubes for polymer-based nanocomposites: a review, *Compos. Part A: Appl. Sci. Manuf.* **41**, 1345-1367.

Manias, E., Stiffer by design, 2007, *Nat. Mater.* **6**, 9-11.

McAllister, M.J., J.-L. Li, D.H. Adamson, H.C. Schniepp, A.A. Abdala, J. Liu, M. Herrera-Alonso, D.L. Milius, R. Car, R.K. Prud'homme, and I.A. Aksay, 2007, Single sheet functionalized graphene by oxidation and thermal expansion of graphite,

Chem. Mater. **19**, 4396-4404.
Mechrez, G., R.Y. Suckeveriene, E. Segal, and M. Narkis, 2014, Polymer/carbon nanofillers films fabricated by latex technology, *Polym. Adv. Technol.* **25**, 1301-1306.
Mezzenga, R. and J. Ruokolainen, 2009, Nanoparticles in the right place, *Nat. Mater.* **8**, 926-928.
Narh, K.A., L. Jallo, and K.Y. Rhee, 2008, The effect of carbon nanotube agglomeration on the thermal and mechanical properties of polyethylene oxide, *Polym. Compos.* **29**, 809-817.
Nikolić, N., M. Sakač, and J. Mastilović, 2011, Effect of buckwheat flour addition to wheat flour on acylglycerols and fatty acids composition and rheology properties, *LWT - Food Sci. Technol.* **44**, 650-655.
Njuguna, J., K. Pielichowski, and S. Desai, 2008, Nanofiller-reinforced polymer nanocomposites, *Polym. Adv. Technol.* **19**, 947-959.
Paine, A.J., W. Luymes, and J. McNulty, 1990, Dispersion polymerization of styrene in polar solvents. 6. Influence of reaction parameters on particle size and molecular weight in poly(N-vinylpyrrolidone)-stabilized reactions, *Macromolecules* **23**. 3104-3109.
Paredes, J.I., S. Villar-Rodil, A. Martínez-Alonso, and J.M.D. Tascón, 2008, Graphene oxide dispersions in organic solvents, *Langmuir* **24**, 10560-10564.
Pei, S. and H.-M. Cheng, 2012, The reduction of graphene oxide, *Carbon* **50**, 3210-3228.
Ramanathan, T., A.A. Abdala, S. Stankovich, D.A. Dikin, M. Herrera-Alonso, R.D. Piner, D.H. Adamson, H.C. Schniepp, X. Chen, R.S. Ruoff, S.T. Nguyen, I.A. Aksay, R.K. Prud'Homme, and L.C. Brinson, 2008, Functionalized graphene sheets for polymer nanocomposites, *Nat. Nanotech.* **3**, 327-331.
Regev, O., P.N.B. ElKati, J. Loos, and C.E. Koning, 2004, Preparation of conductive nanotube–polymer composites using latex technology, *Adv. Mater.* **16**, 248-251.
Sandler, J.K.W., J.E. Kirk, I.A. Kinloch, M.S.P. Shaffer, and A.H. Windle, 2003, Ultra-low electrical percolation threshold in carbon-nanotube-epoxy composites, *Polymer* **44**, 5893-5899.
Shahil, K.M.F. and A.A. Balandin, 2012, Graphene–multilayer graphene nanocomposites as highly efficient thermal interface materials, *Nano Lett.* **12**, 861-867.
Smith, J.G., D.M. Delozier, J.W. Connell, and K.A. Watson, 2004, Carbon nanotube-conductive additive-space durable polymer nanocomposite films for electrostatic charge dissipation, *Polymer* **45**, 6133-6142.
Song, J.P., S.H. Choi, D.-W. Chung, and S.J. Lee, 2021, Latex-based polystyrene nanocomposites with non-covalently modified carbon nanotubes, *Polymers* **13**, 1168.
Stankovich, S., R.D. Piner, X. Chen, N. Wu, S.T. Nguyen, and R.S. Ruoff, 2006, Stable aqueous dispersions of graphitic nanoplatelets via the reduction of exfoliated graphite oxide in the presence of poly(sodium 4-styrenesulfonate), *J. Mater. Chem.* **16**, 155.
Steurer, P., R. Wissert, R. Thomann, and R. Mülhaupt, 2009, Functionalized graphenes and thermoplastic nanocomposites based upon expanded graphite oxide, *Macromol. Rapid Commun.* **30**, 316-327.
Stobinski, L., B. Lesiak, A. Malolepszy, M. Mazurkiewicz, B. Mierzwa, J. Zemek, P. Jiricek, and I. Bieloshapka, 2014, Graphene oxide and reduced graphene oxide studied by the XRD, TEM and electron spectroscopy methods, *J. Electron Spectros. Relat. Phenomena* **195**, 145-154.
Sun, Z., M. Xiao, S. Wang, D. Han, S. Song, G. Chen, and Y. Meng, 2014, Electrostatic shield effect: an effective way to suppress dissolution of polysulfide anions in lithium–sulfur battery, *J. Mater. Chem. A* **2**, 15938.
Šupová, M., G.S. Martynková, and K. Barabaszová, 2011, Effect of nanofillers dispersion in polymer matrices: a review, *Sci. Adv. Mater.* **3**, 1-25.
Sureshkumar, M., H.Y. Na, K.H. Ahn, and S.J. Lee, 2015, Conductive nanocomposites based on polystyrene microspheres and silver nanowires by latex blending, *ACS Appl. Mater. Interfaces* **7**, 756-764.
Tkalya, E., M. Ghislandi, A. Alekseev, C. Koning, and J. Loos, 2010, Latex-based concept for the preparation of graphene-based polymer nanocomposites, *J. Mater. Chem.* **20**, 3035-3039.
Trujillo, M., M.L. Arnal, A.J. Müller, E. Laredo, St. Bredeau, D. Bonduel, and Ph. Dubois, 2007, Thermal and morphological characterization of nanocomposites prepared by in-situ polymerization of high-density polyethylene on carbon nanotubes, *Macromolecules* **40**, 6268-6276.
Wang, G.-F., X.-M. Tao, and R.-X. Wang, 2008, Flexible organic light-emitting diodes with a polymeric nanocomposite anode, *Nanotechnol.* **19**, 145201.
Weber, M. and M.R. Kamal, 1997, Estimation of the volume resistivity of electrically conductive composites, *Polym. Compos.* **18**, 711-725.
Wu, H.P., J.F. Liu, X.J. Wu, M.Y. Ge, Y.W. Wang, G.Q. Zhang, and J.Z. Jiang, 2006, High conductivity of isotropic conductive adhesives filled with silver nanowires, *Int. J. Adhes. Adhes.* **26**, 617-621.
Wu, T.-M. and E.-C. Chen, 2008, Preparation and characterization of conductive carbon nanotube–polystyrene nanocomposites using latex technology, *Compos. Sci. Technol.* **68**, 2254-2259.
Yoo, D., J. Kim, and J.H. Kim, 2014, Direct synthesis of highly conductive poly(3,4-ethylenedioxythiophene):poly(4-styrenesulfonate) (PEDOT:PSS)/graphene composites and their applications in energy harvesting systems, *Nano Res.* **7**, 717-730.
Zhan, C., G. Yu, Y. Lu, L. Wang, E. Wujcik, and S. Wei, 2017, Conductive polymer nanocomposites: a critical review of modern advanced devices, *J. Mater. Chem. C* **5**, 1569-1585.
Zhang, Q., F. Fang, X. Zhao, Y. Li, M. Zhu, and D. Chen, 2008, Use of dynamic rheological behavior to estimate the dispersion of carbon nanotubes in carbon nanotube/polymer composites, *J. Phys. Chem. B.* **112**, 12606-12611.
Zhang, Y., Y.-J. Heo, Y.-R. Son, I. In, K.-H. An, B.-J. Kim, and S.-J. Park, 2019, Recent advanced thermal interfacial materials: a review of conducting mechanisms and parameters of carbon materials, *Carbon* **142**, 445-460.